

Portable optical frequency standard based on sealed gas-filled hollow-core fiber using a novel encapsulation technique

Marco Triches^{1,2}  · Anders Bruschi¹ · Jan Hald¹

Received: 11 June 2015 / Accepted: 10 September 2015 / Published online: 23 September 2015
© Springer-Verlag Berlin Heidelberg 2015

Abstract A portable stand-alone optical frequency standard based on a gas-filled hollow-core photonic crystal fiber is developed to stabilize a fiber laser to the $^{13}\text{C}_2\text{H}_2$ P(16) ($\nu_1 + \nu_3$) transition at 1542 nm using saturated absorption. A novel encapsulation technique is developed to permanently seal the hollow-core fiber with easy light coupling, showing negligible pressure increase over two months. The locked laser shows a fractional frequency instability below 8×10^{-12} for an averaging time up to 10^4 s. The lock-point repeatability over one month is 2.6×10^{-11} , corresponding to a standard deviation of 5.3 kHz. The system is also assembled in a more compact and easy-to-use configuration (*Plug&Play*), showing comparable performance with previously published work. The *real* portability of this technology is proved by shipping the system to a collaborating laboratory, showing unchanged performance after the return.

1 Introduction

During the last 50 years, many high-resolution spectroscopy techniques have been developed based on saturated absorption spectroscopy (SAS) [1–3]. Laser frequency stabilization is a direct application of these Doppler-free spectroscopy techniques, and many frequency-locking schemes have been developed based on them [4, 5]. Since the demonstration of the first photonic band gap guidance in air [6], the hollow-core (HC) fibers are implemented in many different applications such as gas-sensing [7, 8], high-resolution spectroscopy [9–13], nonlinear optics [14, 15], and laser stabilization [16–18]. The unique property of HC fiber to provide diffraction-less light propagation in air over several meters allows the development of compact gas *cells* with longer interaction length. The in-fiber laser frequency stabilization technique is usually based on the combination of SAS with frequency modulation spectroscopy, using a setup similar to the one presented in [3] for the first time.

During the last decade, stabilized laser performance based on a gas-filled HC fiber reference has increased with the improved properties of the HC fiber, aiming to increase the portability of the technology. A portable optical frequency standard that goes beyond the standards commercially available is important in metrology and in many other applications (optical-sensing, geodesy, telecommunication, etc.) that need an accurate and reliable frequency reference outside the laboratory. However, developing a portable and user-friendly optical frequency standard is not free of challenges.

Despite the 10 years elapsed from the first breakthrough demonstration of a gas cell based on sealed filled HC fiber [16], none of the optical frequency standards commercially available are based on this technology. Fabrication

Marie Curie Initial Training Network QTea—Quantum Technology Sensors and Applications, financed by the FP7 program of the European Commission (contract-N MCITN-317485). This work was also funded by the European Metrology Research Programme EMRP (JRP IND14 Frequency). The EMRP is jointly funded by the participating countries within EURAMET and the European Union.

✉ Marco Triches
mt@dfm.dk

¹ Danish Fundamental Metrology, Matematikstorvet 307, 2800 Kongens Lyngby, Denmark

² Department of Photonics Engineering, Technical University of Denmark, Ørstedes Plads 343, 2800 Kongens Lyngby, Denmark

techniques are far from being production-oriented, and long-term performance may be compromised by atmospheric air contamination due to a non-perfect seal. These issues are likely to be the major causes of the absence of HC fiber-based gas cells on the market. In fact, targeting a suitable encapsulation technique that combines a compact and efficient laser-to-HC fiber coupling with a long-lasting seal is not trivial. Most of the results published so far [16, 19–21] are based on splicing a tapered HC fiber to a solid-core single-mode (SM) fiber or multimode (MM) fiber. The typical loss for a SM-to-HC splice is between 2 and 3 dB [22], especially if an angled splice is adopted to reduce the Fresnel reflection in the air–silica interface [23]. Recently published work [24] confirms that the technique of collapsing the photonic crystal to seal the fiber compromises the light coupling, because of the poor core mode matching and the unwanted back-reflections.

Furthermore, the splicing/tapering sealing method requires a dedicated filling technique in order to avoid atmospheric gas contamination, as proposed in [25]: The fiber is filled with a mixture of helium and acetylene at the wanted acetylene partial pressure, but with a total pressure of more than 2000 hPa. The high total pressure limits the gas contamination during the final splicing/tapering step, and subsequently, the helium diffuses through the glass structure. Moreover, no direct measurement of the long-term pressure stability of sealed gas-filled HC fibers systems can be found in the literature. In previously published work [21], the sealed acetylene-filled HC fiber cannot reproduce the performance achieved with similar fibers deployed in a vacuum chamber filled with acetylene [17], both in terms of fractional frequency instability and lock-point repeatability.

In this paper, we present a novel encapsulation technique that combines an outstanding pressure stability (with negligible broadening rate) with a compact design. In a previously published work [18], we explore the laser stabilization performance of several hollow-core photonic crystal fibers (HC-PCFs) placed in a vacuum chamber and filled with $^{13}\text{C}_2\text{H}_2$, demonstrating a fractional frequency instability well below 1×10^{-11} for up to one day of averaging time. The chosen $^{13}\text{C}_2\text{H}_2$ P(16) ($\nu_1 + \nu_3$) line at 1542.3837 nm is the recommended optical transition for the realization of the meter in the telecommunication band [26]. Using the best fiber tested in [18], we develop a prototype of a portable stand-alone optical frequency standard.

The performance is within a factor of three with respect to the results in [18], with a frequency instability one order of magnitude lower than previously published for a sealed HC fiber [21]. The prototype is also assembled in a more user-friendly configuration (*Plug&Play*) showing comparable results with respect to [21], but involving a simpler and more compact detection scheme. The system was shipped

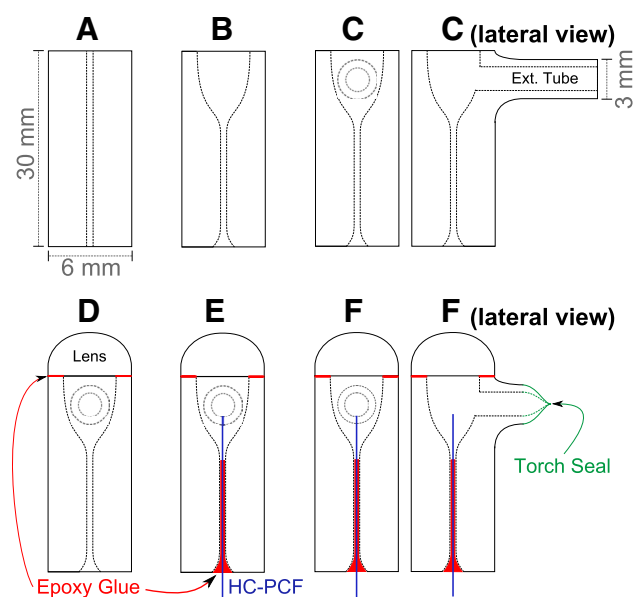


Fig. 1 Description of fabrication steps of the encapsulation method proposed (from a to f)

to a project partner in Finland [27], preserving its performance before/after the shipment and demonstrating the portability of this technology.

2 Materials and methods

2.1 Fiber encapsulation

The novel encapsulation technique is presented in Fig. 1 and consists of six steps, from A to F.

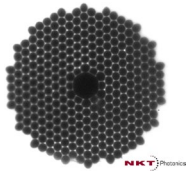
(A): A 40-mm-long borosilicate capillary tube with internal diameter (ID) compatible with the outer diameter of the fiber is used as a ferrule.

(B): Both the ends of the capillary are annealed, and compressed air is blown through the capillary. This procedure expands the ID of the capillary proportionally to the air pressure used. The front facet of the capillary is blown to reduce glass wall thickness to a less than 2 mm, in order to create a small cavity. The back facet is blown to obtain a slightly larger aperture with a smooth surface. This procedure is important for injection of the fiber during assembly without damaging the fiber facet.

(C): During the annealing process of the front facet, a hole is opened on the sidewall of the capillary. A borosilicate tube is fused to the ferrule in order to have lateral access to the small cavity.

(D): The front facet of the ferrule is lapped/polished to an optical finish, and an aspheric lens (Thorlabs A230-C) is glued on top, using a low-outgassing thermal-curing epoxy glue.

Table 1 Summary of the fiber characteristics

Specs	Fiber	Structure
Core (diameter)	7-cell (8.5 μm)	
MFD	5.4 μm	
Coupling (loss)	61 % (2.1 dB)	
PM property	Non-PM	
Modes property	Single mode	
Length	~ 2.7 m	

This fiber has been tested in [18], where it is called C7_S

(E): Once cleaved, the HC-PCF end is injected into the cell (from the back end of the ferrule), and the fiber is glued in position using the epoxy glue. The fiber is positioned at the focal plane of the lens by maximizing the coupling efficiency of a collimated beam launched through the lens. The step is repeated for both the facets using two such ferrules. The fiber is injected into the ferrules without stripping the coating, to improve the mechanical stability of the system.

(F): Both the cells are connected to a vacuum pump and to an acetylene vessel via the lateral tube, in order to purge the fiber before filling. The purging step takes about a week. During this step, a silicone-based vacuum sealant (VacSeal®) is put on the external surface of the epoxy layer to improve the sealing stability. Thanks to the solvent component, the sealant diffuses through the epoxy improving the sealing once cured. The sealant is cured at approximately 60 °C for the entire purging step. Further considerations about the curing process are presented in Sect. 3.1, when the pressure stability of the system is investigated. Once the fiber is purged, the cavity is filled to the low-pressure $^{13}\text{C}_2\text{H}_2$ vapor. A butane flame torch is used to collapse and seal the lateral tube.

This approach combines the easy pressure handling with the desired coupling efficiency (coupling loss below 2.5 dB), in a compact design. The coupling loss is comparable with the optimized free-space coupling configuration reported in Table 1. In this sense, the proposed encapsulation technique aims to combine the goodness of both previously investigated technologies: the high coupling efficiency of the free-space approach, avoiding unwanted Fresnel reflections/etalon effects typical of the splicing, and the size reduction achievable with the splicing techniques. This technique is likely to be useful for any kind of vapor source, reducing the contamination risk in case of potentially harmful vapor (like Rb) and avoiding use of high concentration of buffer gasses.

Moreover, a non-permanent seal with good performance is possible using vacuum grease instead of the epoxy glue, which allows the cell to be cleaned and the fiber to be replaced.

2.2 Fiber specifications

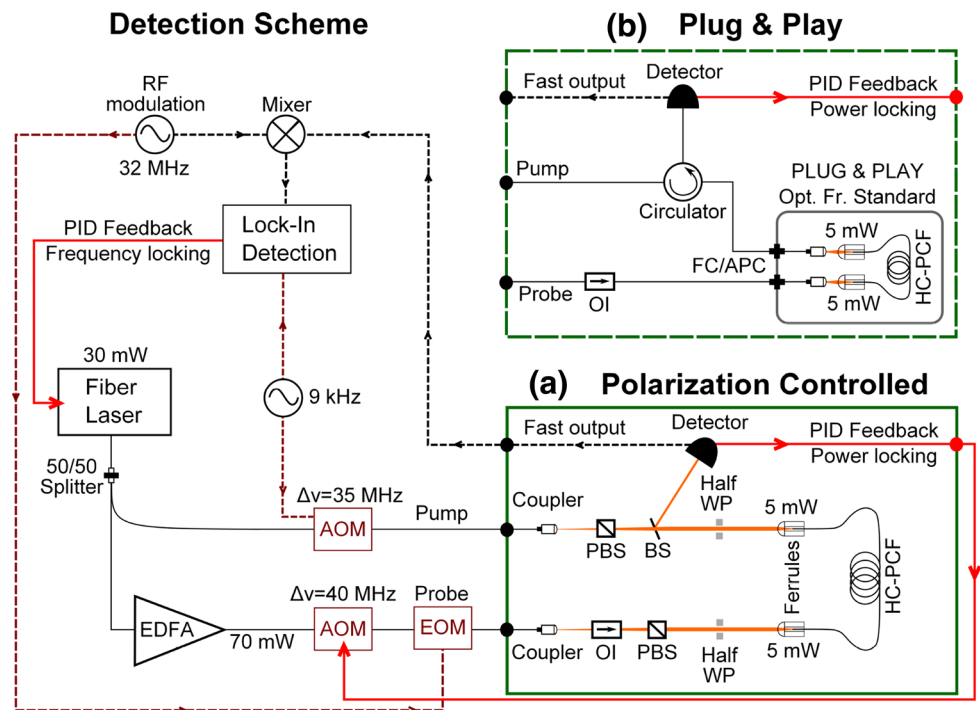
The system is developed using the HC-PCF presented in Table 1, which had the best performance both in terms of fractional frequency instability and lock-point repeatability in a previously published work [18].

After being encapsulated and purged, the fiber is filled with 15 Pa of $^{13}\text{C}_2\text{H}_2$ vapor, which is a factor of two below the optimum pressure as discussed in Sect. 3.2. The resulting lower pressure with respect to the optimum (30 Pa) is due to a mistake in the filling procedure. The optical absorption measured after the sealing confirms that ~ 15 Pa of $^{13}\text{C}_2\text{H}_2$ are loaded into the fiber. In the following discussion, we will refer to sealed gas-filled HC fiber as the *stand-alone system*, i.e., a sealed HC fiber not connected to an external vacuum apparatus.

2.3 Frequency-locking scheme

The same SAS setup described in [18] is used to monitor the performance of the stand-alone system (Fig. 2). A fiber laser source (Koheras E15 Adjustik™) is split into two beams, called pump and probe, respectively. The pump beam is intensity modulated at 9 kHz (and blue-detuned by 35 MHz) using an acousto-optic modulator (AOM). The probe beam is blue-detuned by 40 MHz using a second AOM, after being amplified by an erbium-doped fiber amplifier (EDFA). An electro-optic modulator (EOM) is used to phase modulate the probe at 32 MHz to generate the sidebands needed for frequency modulation spectroscopy. Two different configurations are used to test the performance of the stand-alone system (Fig. 2):

Fig. 2 Schematic layout of the SAS setup. *OI* Optical isolator. *PBS* Polarizing beam splitter. *Half WP* Half-wave plate. *EDFA* Erbium-doped fiber amplifier. *FC/APC* Fiber connector/angle physical contact. *Filled black line* optical fibers. *Dashed line* coaxial cables. **a** Polarization-controlled scheme. **b** *Plug&Play* scheme (*dashed contour*). The detection scheme used is the same for both the configurations



Configuration (a): The pump and probe beams are free space coupled to the sealed HC fiber, and the polarization of the two counter propagating beams is controlled using polarizing beam splitters (PBS) combined with zero-order half-wave plates. Using a beam splitter, the transmitted probe is collected for detection. This configuration is similar to the one described in [21].

Configuration (b): In the *Plug&Play* configuration, the stand-alone optical frequency standard is assembled in a compact and user-friendly configuration: The cells are placed inside a $30 \times 30 \times 15 \text{ cm}^3$ aluminum box, and all the optical components used to control the polarization are removed. Access to the HC fiber inside the box is accomplished via two FC/APC connectors. A fiber-based circulator on the pump arm is used to collect the transmitted probe signal.

In both configurations, the transmitted probe light is coupled to a low noise detector with both AC and DC outputs. The fast signal is used to lock the laser to the optical transition, using a lock-in amplifier combined with a servo loop. The DC output is used to stabilize the probe power via the probe AOM. Both beams have a power of 5.5 mW at the HC fiber input (about 3.3 mW average coupled power). The power used is chosen to reproduce the experimental configuration in [18], in order to easily compare the performance between the stand-alone system and the results reported in [18]. Moreover, two equally intense beams reduce the possible frequency shift of the locking point due to the interaction with any high-order HC fiber modes, as explained in [18]. A small fraction of the laser output is combined with the output of the reference laser (described in [5]), and the resulting beat signal is monitored with a fast photodiode and

a frequency counter. In configuration (a), the polarization of the two counter propagating beams is orthogonal and linear. Despite the fact that fiber is not meant to be polarization maintaining, it is slightly birefringent because of the non-perfectly circular core shape. Therefore, keeping the pump (probe) beam aligned to the *fast* (*slow*) axis of the fiber prevents any instability caused by an unstable polarization configuration in the light–matter interaction, as observed in [18].

In the SAS schemes described, the contribution to the full width at half maximum (linewidth) of the sub-Doppler transition profile due to the acetylene pressure is about 4 MHz [5] for an acetylene pressure of 15 Pa. The absorption of the $^{13}\text{C}_2\text{H}_2$ P(16) line for a 2.7-m fiber at 15 Pa is about 30 % [28]. The transit-time broadening is often the major limiting factor for SAS in HC fibers, because the small mode field diameter (MFD) is one to two orders of magnitude smaller than what is typically used in bulk vapor cell systems. This effect is the main limiting factor associated with this technology, and it is inversely proportional to the MFD. The transit-time broadening contributes to the linewidth with about 26 MHz for the fiber used [12, 29]. The linewidth of the sub-Doppler profile is expected to be around 29–32 MHz at the filling date.

3 Results and discussion

3.1 Pressure stability

In order to evaluate the pressure stability, the linewidth of the sub-Doppler feature is monitored for several months. In this configuration, the fiber laser is offset-locked with

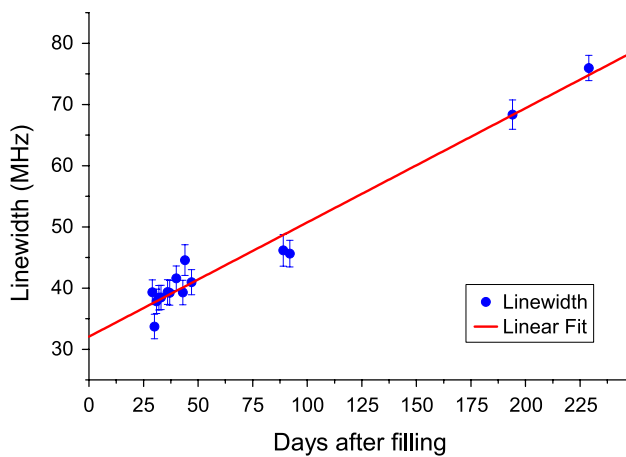


Fig. 3 Sub-Doppler linewidth monitored after filling. The *Plug&Play* system was shipped to a project partner between 100 and 180 days after filling [27]. Each data point is the mean value of multiple measurements of the linewidth. The *error bars* represent the standard deviation associated with each value. The *red line* represents the linear fit of the data

respect to the reference laser [5], and the offset frequency is scanned across the optical transition. The full sub-Doppler optical profile is fitted with a sum of two Lorentzian functions with identical center frequency but individual linewidth and amplitudes. This approach allows us to take into account the contributions to the sub-Doppler feature from both the slow and fast molecules inside the HC fiber, as described in [12]. An example of the sub-Doppler profile of the stand-alone system is reported in [27].

Figure 3 shows the linewidth monitored over 200 days after filling. The system clearly suffers a pressure broadening due to a leak point in the sealing and/or to a source of outgassing inside the cells. The linear regression of the data shows a broadening rate of 186 kHz/day with a standard uncertainty of 9 kHz/day. The estimated linewidth at the filling date is 32 MHz with a standard uncertainty of 1 MHz, which is consistent with the expected value, see Sect. 2.3.

The broadening is due to a pressure increase inside the cell. The most probable scenarios that can cause this effect are as follows:

1. The fiber coating exposed inside the cell is outgassing due to the low pressure.
2. The presence of a leak in the sealing points.
3. The vacuum sealant (VacSeal) applied around the sealing points is not cured completely (see Sect. 2.1). The solvent present in the uncured sealant diffuses through the glue, eventually degassing inside the cell.

In order to discriminate which source is compromising the performance of the system, a vacuum compatible

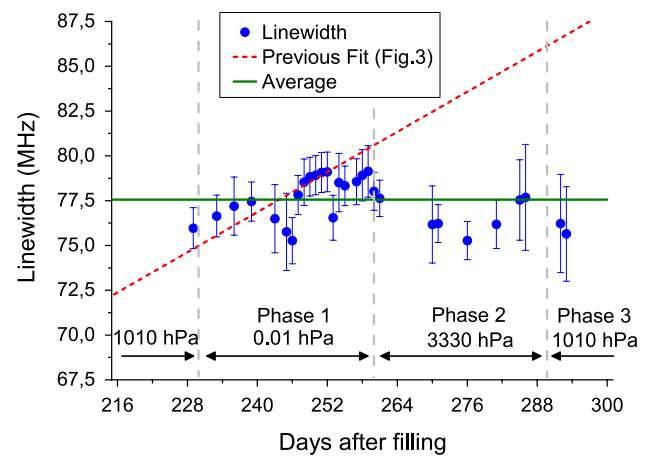


Fig. 4 Pressure test of the stand-alone system. *Red dashed line* previous broadening rate (Fig. 3) given for reference. *Green line* average of the data points. The different phases of the test are highlighted. Each data point is the mean value of multiple measurements of the linewidth of the sub-Doppler feature. The *error bars* represent the standard deviation associated with each value

box with glass windows is assembled. The stand-alone system is placed inside, and the box is connected to a vacuum pump and to a nitrogen vessel (99.99 % purity). The detection scheme is restored to the configuration (a), see Sect. 2.3. In this manner, we can manipulate the pressure of the atmosphere that surrounds the stand-alone system and monitor the linewidth evolution over time. If the broadening is caused by an internal outgassing source, the broadening rate will be independent of applied external pressure. If the sealing has a leak point, the broadening rate will increase/decrease proportionally to the increase/decrease in the external pressure. Moreover, exposing the cells to a low pressure could contribute to cure/evaporate the solvent remaining in the applied sealant layer. The following testing scheme is implemented to the stand-alone system starting from 230 days after filling:

Phase 1 The pressure that surrounds the stand-alone system is lowered down to 0.01 hPa. In this phase, we can neglect the pressure gradient between the cells and the surrounding.

Phase 2 The pressure that surrounds the stand-alone system is increased to 3330 hPa (nitrogen atmosphere).

Phase 3 The box is opened, and the stand-alone system is exposed to the laboratory atmosphere (1010 hPa).

All the three phases are operated at room temperature, and the results are plotted in Fig. 4. The broadening rate registered in the first 230 days is plotted as reference (red dashed line). No statistical evidence of pressure broadening can be observed in any of the three test phases. Instead, the broadening rate stops during the first phase, confirming that the probable cause of broadening experienced in the first 230 days is due to the uncured sealant. It is recommended

by the manufacturer to cure the sealant over about four days at 240 °C, which is not feasible without damaging the fiber. A low-temperature curing approach may cure well the outer layer of the sealant applied, trapping the solvent within the polymer for many months, creating a continuing outgassing problem [30]. This result demonstrates that the sealant can be successfully cured adding a vacuum treatment step for about a couple of weeks instead of an high-temperature exposure. This curing approach can be implemented simultaneously to the fiber purging step, thus solving the issue without increasing the total fabrication time.

The data presented in Fig. 4 show an average linewidth of 77.5 MHz with a standard uncertainty of 0.9 MHz. The acetylene-equivalent pressure of the system is around 200 Pa, calculated using the self-broadening coefficient reported in [5]. This estimate only gives an order of magnitude for the pressure at the end of the test. To give a reliable pressure estimate, the composition of the introduced gasses with their relative broadening coefficients is needed. A linear regression of the data shows a slope of -13 kHz/day with a standard uncertainty of 18 kHz/day. This trend is compatible with a negligible pressure broadening over two months. From the slope and the corresponding uncertainty, we estimate an upper limit for the residual broadening of $+5$ kHz/day, which corresponds to a rate below 2 MHz/year.

3.2 Frequency instability

The performance of the stand-alone system is compared to the reference laser described in [5], both in terms of frequency instability and locking-point repeatability. All the measurements presented here are repeated five times to check the performance repeatability. Figure 5 represents the fractional frequency instability of the beat note between the laser locked to the stand-alone system and the reference laser [5]. The figure includes also a comparison with previously published results for a laser stabilized to a permanently sealed HC fiber filled with acetylene [21]. The free-running laser performance as well as the lower-limit instability achieved with the actual fiber [18] is shown as a reference.

The performance in configuration (a) shows a fractional frequency instability well below 1×10^{-11} for averaging time $1 < \tau < 10^4$ s. The difference between configuration (a) and [18] in terms of instability (a factor of 2.5) can be ascribed to the slightly different configurations involved. The stand-alone system is characterized by a lower filling pressure and slightly shorter fiber (2.7-m fiber filled at 15 Pa) as compared to the fiber used in [18] (3-m fiber filled at 29 Pa). This difference contributes to decrease in the amplitude of sub-Doppler signal by approximately a

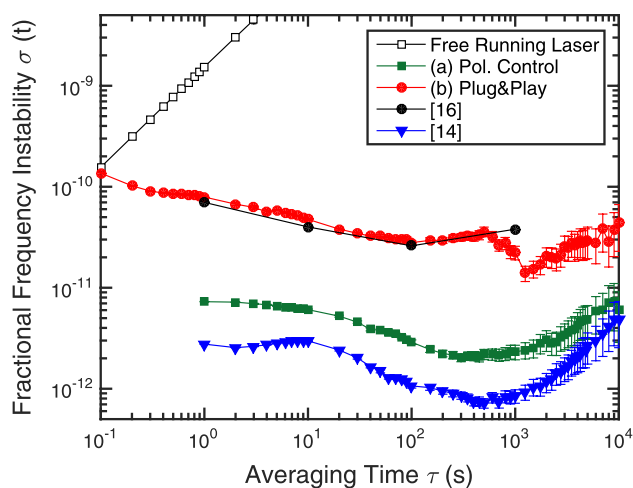


Fig. 5 Fractional frequency instability (Allan deviation) of the two different configurations. *Green filled squares* configuration (a). *Red filled circles* configuration (b). The results published in [21] (*black filled circles*), in [18] (*blue filled triangles*), and the free-running laser performance (*black empty squares*) are plotted for reference

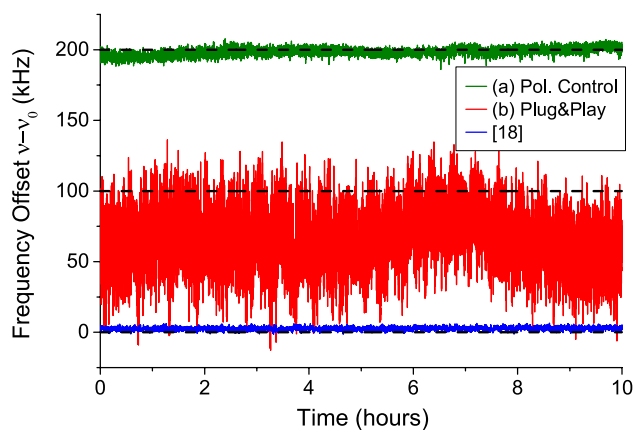


Fig. 6 Frequency of the locked laser over time. The results are plotted with a relative shift of 100 kHz for clarity, after the frequency of the reference laser [5] is subtracted. The best frequency offset performance achieved with the actual HC fiber is plotted for reference [18]. The colors are the same assigned in Fig. 5

factor of two, increasing the instability proportionally in the short timescale. Moreover, the data reported in [18] are acquired in a temperature-stabilized environment, which contributes to lower the instability. These facts allow us to infer that the instability of the stand-alone system (and of the *Plug&Play* as well) can be lowered by a factor of two by optimizing the fiber length and the filling pressure.

The performance in *Plug&Play* configuration (b) is comparable with the one reported in [21], but with a slightly simpler setup, avoiding the fiber-optic polarization controller and with ready-to-use fiber connectors. The importance of the polarization control on SAS in HC fibers has already

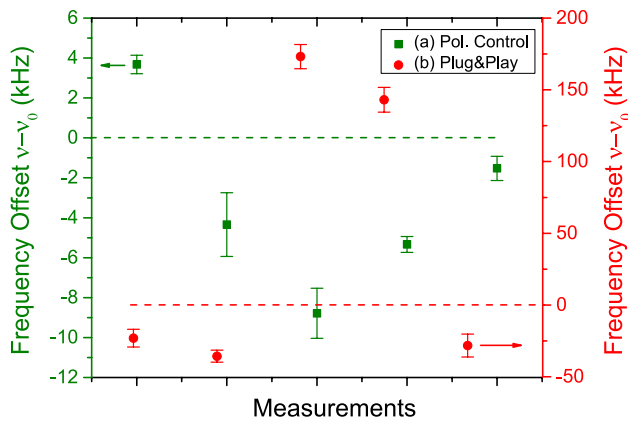


Fig. 7 Lock-point repeatability is presented. *Green squares* configuration (a). *Red circles* *Plug&Play* configuration (b). The *error bars* represent the root mean square value of the measured data. A *dashed line* is added to highlight the zero offset level of each data series

been reported [18, 21], and it is confirmed by the analysis of the frequency offset data in Fig. 6. The frequency difference between the laser locked to the stand-alone system (both in (a) and (b) configurations) and the reference laser [5] is presented. The data are plotted with a relative shift of 100 kHz for clarity. The performance of the actual HC fiber as reported in [18] is plotted for reference.

The frequency fluctuations in the *Plug&Play* configuration (b) with respect to the configuration (a) where the light polarization is controlled are clearly confirming that the absence of polarization control of the launched light is detrimental for the stability of the locked laser. The data in configuration (b) are acquired 60 days after the measurements in configuration (a). During the time elapsed, the linewidth increased by approximately 12 MHz (about 30 % increase) because of the broadening rate. This effect gives a small contribution to the increased instability of the *Plug&Play* system with respect to the configuration (a). The increased instability is mainly ascribed to the absence of polarization control (factor of 7.5) with a minor contribution due to the increased linewidth (factor of 1.3).

Finally, the lock-point repeatability is measured on five different days for both configurations (Fig. 7) over one week. In configuration (a), the stand-alone system shows an average shift of -3.3 kHz with respect to the reference, with a standard deviation of 5.3 kHz, which is comparable with the results we reported in [18]. In the *Plug&Play* configuration (b), the system shows an average shift of $+46$ kHz, with a standard deviation of 103 kHz. This analysis confirms the importance of the polarization control on the light launched into the HC fiber. In order to preserve the outstanding stability/repeatability observed in configuration (a), suitable oriented polarization maintaining fibers can be implemented in the pump/probe arm.

4 Conclusion

We have developed a stand-alone optical frequency standard based on a portable compact gas cell made of a sealed HC fiber filled with $^{13}\text{C}_2\text{H}_2$. The performance of the novel encapsulation technique is investigated, and the pressure stability is characterized over almost a year. No pressure increase is observed over the last 60 days, with the residual broadening rate having an upper limit below 2 MHz/year. To our knowledge, this result demonstrates the long-lasting pressure stability of a sealed gas-filled HC fiber for the first time, solving a crucial technical issue for a future commercialization of similar systems. The stand-alone system is tested in terms of fractional frequency instability showing an Allan deviation below 8×10^{-12} for an averaging time up to 10^4 s (in a polarization-controlled configuration). The frequency of the lock point is repeatable to ± 5.3 kHz (standard deviation over five measurements), resulting in the most stable and accurate laser system locked to a permanently sealed acetylene-filled HC fiber published so far [21]. The system is also assembled in a user-friendly configuration (*Plug&Play*) that shows comparable performance with respect to previously reported results [21], but involving a simpler detection setup. The *Plug&Play* optical frequency standard fits in a box of $30 \times 30 \times 15$ cm³, equipped with fiber connectors. The system was also shipped to partners in Helsinki with unchanged performance before/after the shipment, proving the real portability of the optical frequency standard. Future improvements will address the optimization of the main parameters such as gas pressure, fiber length, and saturation power. Further reduction in physical size will be addressed as well.

Acknowledgments A thanks to NKT Photonics for providing the special fiber used in the papers published so far. A special thanks also to Jan P. Scholer for the practical realization of the glass cells and to Philip G. Westergaard for the feedback received during the cell testing.

References

1. C. Wieman, T.W. Hänsch, Phys. Rev. Lett. **36**(20), 1170 (1976)
2. F.V. Kowalski, W.T. Hill, A.L. Schawlow, Opt. Lett. **2**(5), 112 (1978)
3. J.L. Hall, Appl. Phys. Lett. **39**(9), 680 (1981)
4. C.S. Edwards, H.S. Margolis, G.P. Barwood, S.N. Lea, P. Gill, W.R.C. Rowley, Appl. Phys. B **80**(8), 977 (2005)
5. J. Hald, L. Nielsen, J.C. Petersen, P. Varming, J.E. Pedersen, Opt. Express **19**(3), 2052 (2011)
6. R.F. Cregan, B. Mangan, P. Russell, J. Knight, P. Roberts, D. Allan, Science **285**(5433), 1537 (1999)
7. T. Ritari, J. Tuominen, H. Ludvigsen, J.C. Petersen, T. Sørensen, T.P. Hansen, H.R. Simonsen, Opt. Express **12**(17), 4080 (2004)
8. W. Jin, Y. Cao, F. Yang, H.L. Ho, Nat. Commun. **6**, 6767 (2015)
9. R. Thapa, K. Knabe, M. Faheem, A. Naweed, O.L. Weaver, K.L. Corwin, Opt. Lett. **31**(16), 2489 (2006)

10. S. Ghosh, J.E. Sharping, D.G. Ouzounov, A.L. Gaeta, *Phys. Rev. Lett.* **94**(9), 093902 (2005)
11. S. Ghosh, A.R. Bhagwat, C.K. Renshaw, S. Goh, A.L. Gaeta, B.J. Kirby, *Phys. Rev. Lett.* **97**(2), 023603 (2006)
12. J. Hald, J.C. Petersen, J. Henningsen, *Phys. Rev. Lett.* **98**(21), 213902 (2007)
13. C. Perrella, P.S. Light, T.M. Stace, F. Benabid, A.N. Luiten, *Phys. Rev. A* **85**, 12518 (2012)
14. A.R. Bhagwat, A.L. Gaeta, *Opt. Express* **16**(7), 5035 (2008)
15. P.S.J. Russell, P. Hölzer, W. Chang, A. Abdolvand, J.C. Travers, *Nat. Photonics* **8**(4), 278 (2014)
16. F. Benabid, F. Couny, J.C. Knight, T.A. Birks, P.S.J. Russell, *Nature* **434**(7032), 488 (2005)
17. K. Knabe, S. Wu, J. Lim, K.A. Tillman, P.S. Light, F. Couny, N. Wheeler, R. Thapa, A.M. Jones, J.W. Nicholson, B.R. Washburn, F. Benabid, K.L. Corwin, *Opt. Express* **17**(18), 16017 (2009)
18. M. Triches, M. Michieletto, J. Hald, J.K. Lyngsø, J. Lægsgaard, O. Bang, *Opt. Express* **23**(9), 11227 (2015)
19. C. Hensley, D.H. Broaddus, C.B. Schaffer, A.L. Gaeta, *Opt. Express* **15**(11), 6690 (2007)
20. P.T. Marty, J. Morel, T. Feurer, *J. Light. Technol.* **28**(8), 1236 (2010)
21. C. Wang, N.V. Wheeler, C. Fourcade-Dutin, M. Grogan, T.D. Bradley, B.R. Washburn, F. Benabid, K.L. Corwin, *Appl. Opt.* **52**(22), 5430 (2013)
22. R. Thapa, K. Knabe, K.L. Corwin, B.R. Washburn, *Opt. Express* **14**(21), 9576 (2006)
23. F. Couny, F. Benabid, P. Light, *IEEE Photonics Technol. Lett.* **19**(13), 1020 (2007)
24. P.S. Light, J.D. Anstie, F. Benabid, A.N. Luiten, *Opt. Lett.* **40**(12), 2703 (2015)
25. P.S. Light, F. Couny, F. Benabid, in *Conf. Lasers Electro-Optics/Quantum Electron. Laser Sci. Conf. Photonic Appl. Syst. Technol.* (Optical Society of America, Baltimore, Maryland, 2007), p. CThKK4
26. R. Felder, *Metrologia* **42**(4), 323 (2005)
27. J. Seppä, M. Merimaa, A. Manninen, M. Triches, J. Hald, A. Lassila, *I.E.E.E. Trans, Instrum. Meas.* **64**(6), 1595 (2015)
28. M. Kusaba, J. Henningsen, *J. Mol. Spectrosc.* **209**(2), 216 (2001)
29. V.S. Letokhov, *High-Resolution Laser Spectroscopy, Topics in Applied Physics*, vol. 13 (Springer, Berlin, Heidelberg, 1976)
30. VacSeal Inc. Vacseal High Vacuum Leak Sealant—Curing Protocols. <http://www.2spi.com/catalog/vac/vacseal-curing-protocols.html>